Platinum surface instabilities and their impact in electrochemistry

Valls Mascaro, F.

3 Step Bunching Instability and its Effects in Electrochemistry: Pt(111) and its Vicinal Surfaces

Abstract

The atomic-scale surface structure plays a major role in the electrochemical behavior of a catalyst. The electrocatalytic activity towards many relevant reactions, such as the Oxygen Reduction Reaction on platinum, exhibits a linear dependency with the number of steps until this linear scaling breaks down at high step densities. Here we show, using Pt(111)-vicinal surfaces and *in-situ* Electrochemical Scanning Tunneling Microscopy (EC-STM), that this anomalous behavior at high step densities has a structural origin, and is attributed to the bunching of closely spaced steps. While Pt(554) presents parallel single steps and terrace widths that correspond to its nominal, expected value, most steps on Pt(553) are bunched. Our findings challenge the common assumption in electrochemistry that all stepped surfaces are composed by homogeneously spaced steps of mono-atomic height and can successfully explain the anomalous trends documented in the literature linking step density to both activity and potential of zero total charge.

3.1 Introduction

Stepped platinum single crystals are widely used in electrochemistry to study the unique reactivity of step sites. Low-Energy Electron Diffraction, He-beam diffraction, and STM studies in ultra-high vacuum (UHV) confirmed that Pt(111)-vicinal surfaces such as Pt(997) prepared by sputtering and annealing are stable at moderate temperatures as long as oxygen is not present whilst the sample is hot [1–4]. Unfortunately, there is scarce work on the atomic-scale characterization of stepped surfaces when prepared by flame-annealing (in air) and cooled down in a reducing atmosphere, which is the typical methodology followed in electrochemistry [5]. Herrero et al. showed that Pt(10 10 9) and Pt(11 10 10) (both with steps along a direction equivalent to [110], but with the former having {111}, and the later having {100} microfacets) present their nominal structures if an Ar + H_2 mixture is used while cooling down the samples [6]. As a result, it is often assumed in single-crystal electrochemistry studies that all stepped surfaces are composed of parallel running monoatomic-height steps.

This assumption, however, is inconsistent with many experimental observations that show a dissimilar relation to the density of step (or step-related) sites among different Pt(111)-vicinal surfaces. For example, the potential at which the total charge is zero (E_{pztc}) decreases linearly with the step density, as expected, but only until a certain critical value, from on which it deviates significantly [7]. Similarly, the linear scaling between the Oxygen Reduction Reaction (ORR) activity and the step density breaks down for stepped surfaces with very small terraces [8, 9]. This phenomenon suggests a structural difference of the steps depending on the terrace width, despite the lack of supporting evidence in the literature.

In this article we offer an explanation for this anomalous behavior. Using EC-STM we show that Pt(554) exhibits exclusively single, monoatomic-height steps, while a stepped surface with theoretically narrow terraces, such as Pt(553), shows mainly double-height (bunched) steps and terraces with twice the nominal width. Based on this observation, we quantitatively show, on the example of the E_{pztc} and the ORR activity, that step bunching can successfully explain the anomalous behavior of surfaces with high step density.

3.2 Experimental

Electrochemistry. We recorded the cyclic voltammograms in a glass cell that we cleaned first with an acidic potassium permanganate solution and then with diluted piranha, before finally boiling it five times in ultrapure water (> 18.2 MΩ cm, Millipore Milli-Q). For the measurements, we used a reversible hydrogen electrode (RHE) as the reference and a Pt wire (MaTeck, Germany) as the counter electrode. Our working electrode was a high quality (99.999 % purity and polished < 0.1°) platinum single crystal, either a Pt(111) (Surface Preparation Laboratory, The Netherlands) or a (111)-vicinal surface with (111) steps (MaTeck, Germany). The latter can be described with the notation Pt(s)[n(111) x (111)], where n is the number of atomic rows on a single terrace. Before the measurements, we etched the platinum sample electrochemically (125 cycles at 50 Hz, ± 2 V versus Pt) in an

acidified 2.5 M $CaCl_2$ solution. Subsequently, we flame annealed it (3 min at ≈ 1250 K) and cooled it down in a 1:4 H_2/Ar mixture. We repeated this treatment three times, with the last annealing step at a slightly lower temperature (≈ 50 K lower) in order to deplete the surface from contamination coming from the bulk. We performed all the cyclic voltammograms in an Ar-purged 0.1 M $HClO_4$ solution (Merck Suprapur), using a potentiostat from Bio-Logic (VSP-300).

Electrochemical Scanning Tunneling Microscopy. We recorded the STM images with a home-build EC-STM [10, 11]. We used an RHE and a Pt coil as reference and counter electrodes, respectively, while the working electrode was either Pt(554) or Pt(553) with which we also recorded the cyclic voltammograms. We made the STM tips by electrochemically etching of a $Pt_{90}Ir_{10}$ wire (Goodfellow), and we coated them with electrophoretic paint (Clearclad HSR) and polyethylene to minimize the faradaic contributions in the tunneling current. Before every measurement, we cleaned all the glassware and pipes following the procedure described in Ref. [12] and we de-aerated the electrolyte (0.1 M $HClO_4$) with N_2 for at least 3 hours.

3.3 Thermodynamics of Stepped Surfaces

At thermodynamic equilibrium, the surface morphology always conforms to the one with the lowest free energy. For a high Miller-index surface, the surface free energy at a temperature T is given by [13]:

$$f_{total}(T) = f_{terr}(T) + f_{step}(T)\,\frac{1}{L} + B_{step}(T)\,\frac{1}{a\,L^3} \tag{3.1}$$

where f_{terr} corresponds to the free energy of the terraces and f_{step} is the free energy of the steps, which is divided by the terrace width (L) in order to account for the step density. The third term describes the interactions between steps, where B_{step} is an interaction coefficient and a the unit step length: a = 2.78 Å.

The temperature dependence is specially important for f_{step}, as all steps are rough at any $T > 0$ K: thermally-activated kinks form and enable the steps to meander, thereby increasing their entropy and lowering their free energy f_{step} according to [14]:

$$f_{step}(T) = f^0_{step} - \frac{2\,k_B\,T}{a}\,exp(\frac{-f^0_{kink}}{k_B\,T}) \tag{3.2}$$

where f^0_{step} and f^0_{kink} are the formation energies of a unit step length and a kink site, respectively, while k_B is the Boltzmann's constant. Note that at a high enough T the exponential term in equation 3.2 becomes practically equal to 1, which can lead to $f_{step} < 0$, i.e. the surface can form steps spontaneously, describing the 3D roughening transition [15].

Step meandering is, however, hindered by the step-step interaction, which has three different components. The first one is an entropic repulsion originating from the geometric confinement of a step in between its two neighbors [16, 17]. The second one is an electrostatic interaction between electric dipoles that form at step edges due to the Smoluchowski effect [18, 19], which goes hand-in-hand with an elastic interaction [20–23]. Unlike the

entropic repulsion, the electrostatic and elastic interactions are always repulsive for neighboring steps of the same type (ascending or descending), while they can be either repulsive or attractive for opposite type of steps, depending on the strength of the dipole moment parallel to the surface [14]. In any case, all three contributions to the step-step interaction usually decay with L^{-2} [19, 24]. Scaling this factor to units of energy/area, we obtain the L^{-3} dependency that is reflected in the third term of equation 3.1.

In the next section we first present our results on the characterization of Pt(554) and Pt(553), before we discuss the origin of the step bunching instability based on the thermodynamic description given above.

3.4 Surface Characterization

Figure 3.1 (**a** and **b**) shows 3D rendered EC-STM images of a Pt(554) surface and a Pt(553) surface recorded at constant sample and tip potentials, $U_s = 0.1$ V and $U_t = 0.15$ V, respectively, which we processed on the terrace planes to bring out the natural tilt of each sample (see Appendix B for details). When comparing both images, one realizes that the average separation between the steps, the brighter parallel lines, is similar on both surfaces, which is supported by the corresponding height lines shown in Fig. 3.1 (**c** and **d**): the terraces selected on Pt(554) and Pt(553) measure 23.1 Å and 23.9 Å in width, respectively. This is surprising, as Pt(553) naturally has double the step density of Pt(554). In fact, the nominal terrace widths are 22.4 Å and 10.4 Å, respectively, as given by the ball model equation:

$$L = \frac{\sqrt{3}}{2}\, d\,(n-1) + \frac{\sqrt{3}}{3}\, d \tag{3.3}$$

where d is the distance between two close-packed platinum atoms and n is the number of atom rows in a single terrace (n = 10 for Pt(554) and n = 5 for Pt(553)). As the steps can not simply vanish, because the natural surface orientation must be always preserved, the only possible explanation for the doubling of the terrace width on Pt(553) is that the steps bunch together in pairs, as shown in Fig. 3.2. Evidence for this is the step height of 4.48 Å measured in Fig. 3.1d, which is twice the theoretical (111) step height of 2.27 Å.

To quantify our observation statistically, we traced over 50 randomly-chosen height lines from which we measured the step heights and terrace widths for both Pt(554) and Pt(553), analyzing several STM images that were recorded in different experiments (see Appendix B). Figure 3.3a shows the resulting terrace width distribution for Pt(554). Its Gaussian shape indicates the existence of a repulsive interaction between the closely spaced steps, as opposed to an asymmetric peak that would be characteristic for freely fluctuating steps [13, 16]. The width of the distribution, often defined as its standard deviation (σ), depends on the interplay between f_{step} and B_{step}: a lower B_{step}, lower f^0_{kink}, or a higher T results in a broader peak, as it costs less energy for the steps to wander further away from the midway position between their neighbors. From the Gaussian fit in red, we obtain $\sigma = 4.2$ Å, which is higher than the $\sigma = 2.9$ Å reported for Pt(997) in vacuum [4]. This is what we would expect, as the terraces on Pt(554) are one atom row wider than on Pt(997), resulting in a lower step-step repulsive interaction. However, (part of) this difference might be also attributed to the screening of the dipole by the electrolyte. The center of the Gaussian distribution is

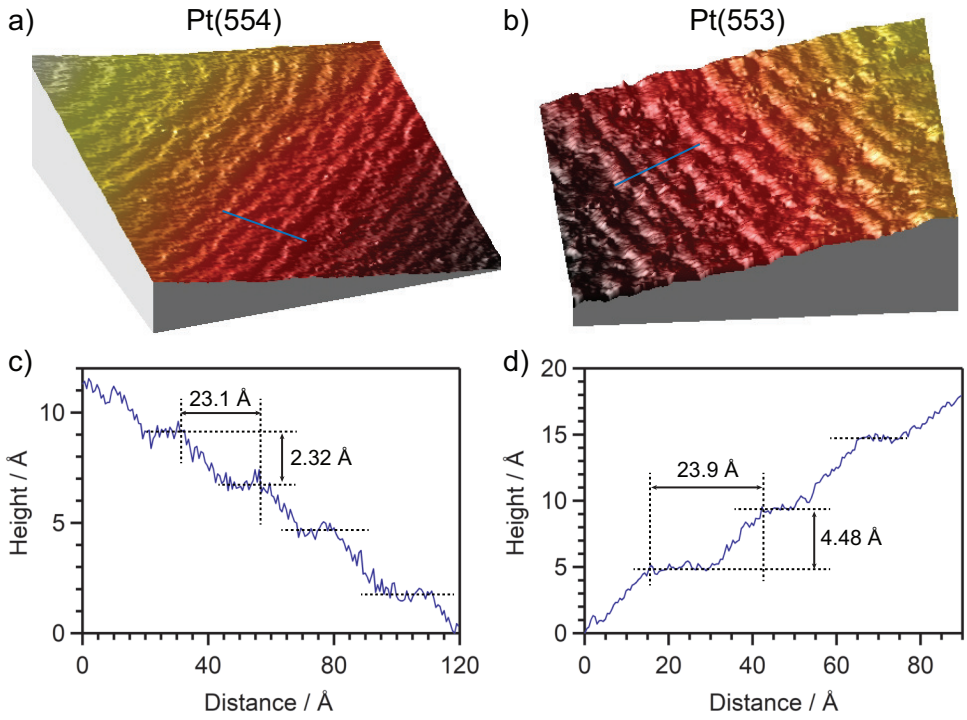

Figure 3.1: EC-STM Measurements of Pt(111)-Vicinal Surfaces. 3D rendered EC-STM images of **(a)** Pt(554) and **(b)** Pt(553), recorded in 0.1 M $HClO_4$ with U_s = 0.1 V and U_t = 0.15 V. Both images are 48 x 48 nm^2. The blue lines crossing the steps on Pt(554) and Pt(553) indicate the positions of the corresponding height lines shown in **(c)** and **(d)**. Note that the step height on Pt(553) is twice the one on Pt(554) and that both surfaces show an almost equal terrace width, although it should be theoretically 46 % smaller on Pt(553).

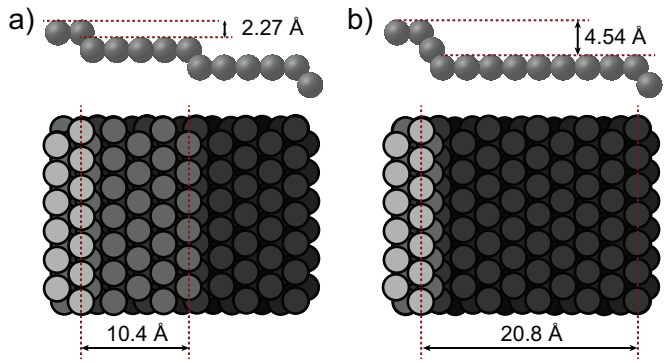

Figure 3.2: Ball Model of a Pt(553) Surface: (a) with single steps, **(b)** with double, bunched steps.

located at 21.9±0.9 Å, which agrees with the theoretical terrace width of 22.4 Å. Moreover, Fig. 3.3b exhibits only one peak in the distribution indicating that the steps on Pt(554) have mono-atomic height.

In contrast, the terrace width distribution on Pt(553), shown in Fig. 3.3c, reveals not only one but three peaks, centered at 11.3±0.5 Å, 20.6±0.5 Å, and 30±1 Å. These peaks correspond to terraces with nominal, double, and triple terrace widths, respectively, thus pointing to the presence of double and triple steps. This again is supported by the step height distribution in Fig. 3.3d, which shows also three different peaks, centered at around 2.25 Å (monoatomic step-height), 4.50 Å (double step-height), and 6.75 Å (triple step-height).

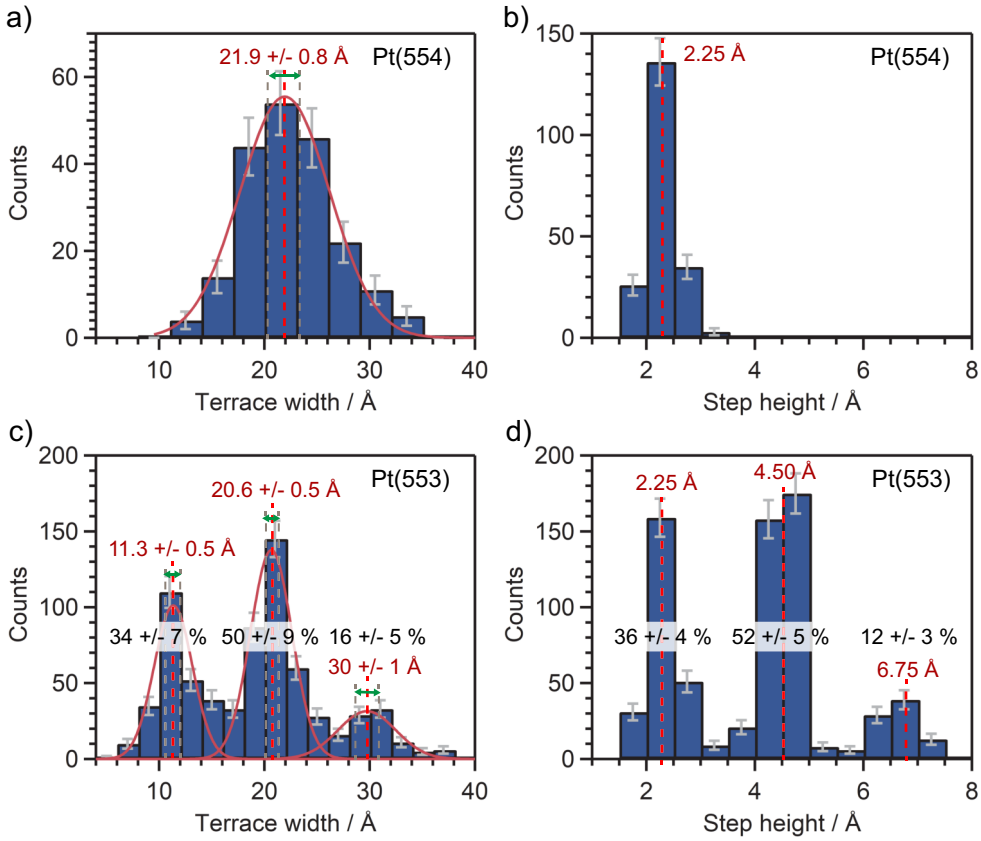

Figure 3.3: Statistical Analysis of the Surface Structure. **(a)** and **(b)** show the terrace width and step-height distributions of Pt(554), while **(c)** and **(d)** show the ones of Pt(553). The values in red and the red dashed lines indicate the center of each peak. For **(a)** and **(c)**, we obtained these values from Gaussian fits, with which we deconvoluted the peaks in the case of Pt(553). The statistical errors shown with gray error bars on each bin lead to uncertainties on the center values (green arrows) as well as on the percentages of single, double, and triple steps, which are reported in black on top of the corresponding peak.

From the percentages indicated on each peak in Fig. 3.3c and Fig. 3.3d, we extracted the corresponding averaged percentages of single (35±4 %), double (51±5 %), and triple (14±3 %) steps on Pt(553). We conclude that, while Pt(554) shows exclusively single steps and a terrace width around its nominal value, more than 65% of the steps on Pt(553) are bunched.

3.5 Origin of the Step Bunching Instability

Whether a vicinal surface undergoes step bunching depends on the delicate balance between f_{step} and B_{step}, which may result in a lower total free energy f_{total} for the bunched configuration. Figure 3.4a shows f_{total} with and without the repulsive step-step interaction, calculated with equations 3.1 and 3.2 and plotted versus the terrace width. One can observe that the dependence of f_{total} on the terrace width is mainly given by f_{step}/L up to narrow terraces (n = 8), below which the step-step interaction starts to play an increasingly significant role.

The surface configuration with double steps does not only have terraces with twice of the nominal terrace width, but also a different f_{step} and B_{step} compared to single steps, resulting in a different f_{total}. Figure 3.4b shows the energy ratio between a surface with double steps and one with single steps calculated at T = 1300 K, which is around 100 K below the maximum temperature reached during our flame-annealing. As surface diffusion drops exponentially with temperature, we estimate that upon further temperature decrease during the cooling down the step configuration becomes *frozen*. As an approximation, we also assumed for this calculation that the formation and kink energies of a double step ($f^0_{double\,step}$ and $f^0_{double\,kink}$, respectively) are exactly two times f^0_{step} and f^0_{kink} [27]. Moreover, we derived that the step-step interaction of double steps ($B_{double\,step}$) is 1.34 times larger than the one of single steps, see Appendix B, where we also show the temperature dependency of the energy ratio.

Figure 3.4b shows that, for our case, stepped surfaces with a terrace width larger than 8 atomic rows are expected to be stable, while those with equal or narrower terraces decrease the total free energy by the formation of step bunches. This is due to the lowering of the step-step repulsion when doubling the terrace width, as not only the step-step interaction term scales with L^{-3} (while the second term in equation 3.1 goes with L^{-1}) but also because $B_{double\,steps} < 2\ B_{step}$ [13, 28]. Although this result is only indicative, as we used some assumptions and values from vacuum studies, it explains why Pt(554) has single steps while Pt(553) mainly has double steps. Moreover, step bunching could also elucidate why, according to Surface X-Ray Diffraction studies, flame-annealed Pt(311) and Pt(331) surfaces do not present their expected, nominal structure [29, 30].

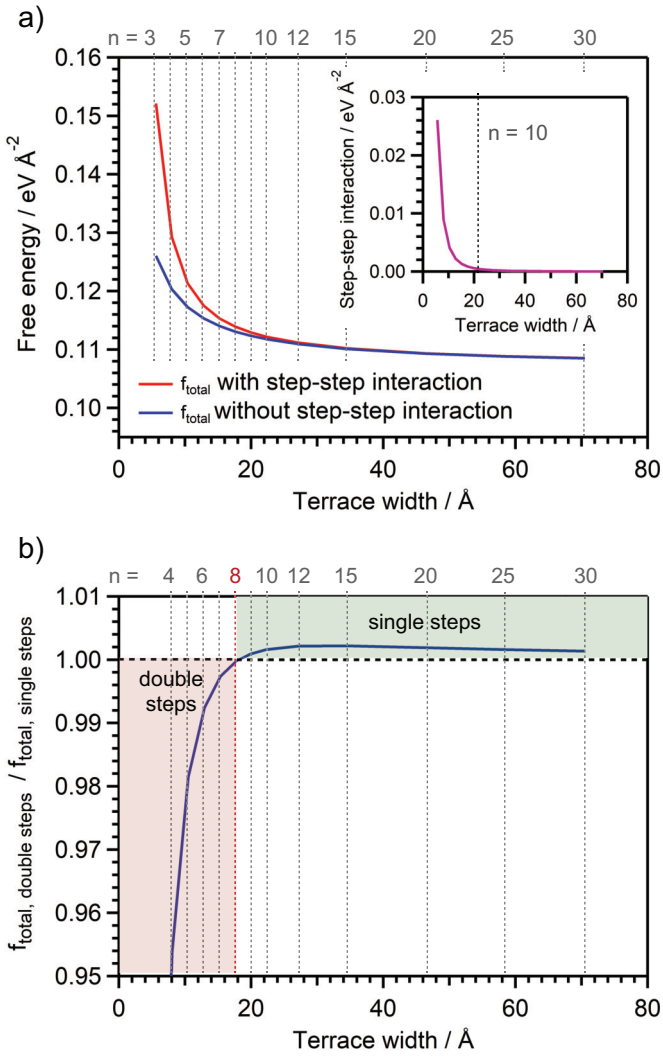

Figure 3.4: Thermodynamics of Step Bunching. **(a)** f_{total} with step-step interaction (red), f_{total} without step-step interaction (blue), and step-step interaction (inset, in purple) versus the terrace width for T = 1300 K. For the calculations, we used equations 3.1 and 3.2, with f_{terr} = 1.07 eV Å^{-2} from Ref. [25] and the values of f^0_{step} = 0.120 eV Å^{-1} and f^0_{kink} = 0.206 eV from Ref. [26]. We extracted the step interaction parameter B_{step} = 12.76 eV Å^2 from the one reported in Ref. [25], which we extrapolated to match with our temperature (see Appendix B). **(b)** Surface free energy ratio between configurations with double and single steps. To calculate the surface free energy for the double steps we reasonably approximated $f^0_{double\,step}$ = 2 x f^0_{step} = 0.240 eV Å^{-1} and $f^0_{double\,kink}$ = 2 x f^0_{kink} = 0.412 eV. We extracted $B_{double\,step}$ = 17.11 eV Å^2 by scaling B_{step} with the ratio of the dipole moments of double steps and single steps, as explained in the Appendix B.

However, as we performed the flame-annealing in air and immediately transferred the sample for cooling down into a glass cylinder with an Ar + H_2 mixture, we can not discard the presence of small amounts of oxygen that could have lowered $f_{double\,step}$, thereby inducing the step bunching instability [1–4, 6]. This would explain why Lang and Blakely observed with LEED that even platinum stepped surfaces with a terrace width of only 3 atomic rows were stable if prepared in UHV [1, 2], although it has also been shown that Pt(997) with a terrace width of 9 atomic rows is prone to faceting, and not step bunching, in the absence of oxygen [4]. Future work is needed to check whether a different preparation method such as induction-annealing, which avoids exposure to air, would result in the nominal Pt(553) surface.

Finally, we can discard that the surface morphology on Pt(553) changes significantly with time while in the EC-STM, which reinforces our statement that the step bunches are formed during sample preparation with enhanced step mobility. Moreover, we observed the same step bunched structure on Pt(553) at least at two applied potentials: 0.1 V, where H covers the surface, and 0.4 V in the double layer region, where nothing is specifically adsorbed on the surface (see Appendix B). This indicates either that both the hydrogen adsorbed and the clean surface preserve the energetics of the most (thermodynamically) stable structure or that the surface is kinetically *frozen* at room temperature and thus visible changes do not occur within the time-span of our measurements. Our results differ from the ones reported in Refs. [31, 32] with a flame-annealed Ag(19 19 17) submerged in a $CuSO_4$ solution. These showed not only that the density of step bunches on this surface increases with time, but also that this increase occurs faster the higher the applied potential [33]. This indicates that the Ag(19 19 17) surface, as measured, did not reach thermodynamic equilibrium, and that surface diffusion at room temperature is still high enough for step rearrangement. Alternatively, the chemisorption of sulfate or copper deposition as well as alloy formation could have also had an important role [34].

3.6 Effects of Step Bunching in Electrocatalysis

Figure 3.5a shows the hydrogen desorption region from Cyclic Voltammograms (CVs) of Pt(111) and Pt(111)-vicinal surfaces with (111) steps in 0.1 M $HClO_4$. All stepped surfaces present a broad feature below 0.4 V and a sharp peak at around 0.13 V, which relate to terrace and step sites, respectively [35]. Pt(553) and Pt(221) show, in addition, an extra peak at around 0.185 V that was previously attributed to hydrogen desorption from narrow terraces [36]. However, we know now that it is related to hydrogen desorption and its (partial) replacement with hydroxide at step bunches, as discussed in detail in Chapter 4. A similar peak is also observed on Pt(110)-vicinals with (111) steps [37], which supports further our new insights. Pt(775) does not show this feature, but the potential shift of the single step peak (see Appendix B) suggests that also this surface exhibits (some) step bunching.

Step bunching also affects E_{pztc}. As E_{pztc} is closely related to the work function, one expects a linear decrease of E_{pztc} with the step density according to [14, 32, 38–40]:

$$\Delta E_{pztc}(\tfrac{1}{L}) = E_{pztc,\,stepped\,surface} - E_{pztc,(111)} = -\frac{p_z}{\epsilon_0\, a\, L} \tag{3.4}$$

where ϵ_0 is the vacuum dielectric constant and p_z the dipole moment at the steps. However, the red curve in Fig. 3.5b (data extracted from Refs. [7,41]) shows that the initial linear dependency of E_{pztc} with step density starts to deviate for n ≤ 7. This phenomenon was previously attributed to the decay of p_z due to the interference of the stress and electrical fields between close-spaced steps [42]. Evidently, as we now know that close spaced steps bunch, resulting in wider terraces, the real explanation must be different. Mainly, step bunching results in a decrease of the ratio p_z/L, as L is doubled but $p_{z,\,double\,step} << 2\,p_{z,\,single\,step}$ [28]. This leads to a higher E_{pztc} than expected.

Figure 3.5b shows in blue the local E_{pztc} at steps (data extracted from Ref. [43]), which is constant at low step densities but starts increasing at n = 7. As step bunches have a different p_z than single steps, this again suggests that the onset of step bunching starts with Pt(775).

Subsequently, we used both curves in Fig. 3.5b, our measured percentage of bunched steps on Pt(553), and equation 3.4 to calculate $p_{z,\,double\,step}$. Knowing that $p_{z,\,single\,step}$ = 0.14 D (in 0.1 M $HClO_4$) [7] and assuming that $p_{z,\,triple\,step} \approx p_{z,\,double\,step}$, we obtain $p_{z,\,double\,step}$ = 0.168 D and $p_{z,\,double\,step}$ = 0.172 D from the two curves, respectively. This means that the dipole moment of the double step is only ≈ 21 % larger than the one of the corresponding single step. To further confirm this, we use the average value of $p_{z,\,double\,step}$ = 0.170 D together with the measured percentage of bunched steps and estimate E_{pztc} for Pt(553) (drawn with the purple diamond), which is close to the value measured. The even greater deviation for Pt(221) and Pt(331) is most likely due to a larger fraction of triple (and maybe even higher order) steps formed to minimize the higher step-step repulsion.

On another topic, it is well known that the ORR in acidic media is most active at the concave sites situated at the lower step edge, where the OH_{ad} intermediate binds weaker than on the (111) terraces [44, 45]. Consequently, one would expect the ORR activity to increase (almost) linearly with the number of these concave sites, and thus with step density (the effects of the Smouluchowski relaxation have a higher order dependency with the step separation, and thus are less significant [18–22]). However, Fig. 3.5c shows in red (data extracted from Refs. [8, 9]) that the ORR half-wave potential ($E_{1/2}$), an activity descriptor, increases linearly with step density only until n < 7.

As we know now that Pt(775), Pt(221), and Pt(331) undergo step bunching, this reduces the amount of lower step edge sites in approximation by a factor 1/2 if all steps would simply bunch into pairs (see Fig. 3.2). As these are the most active sites for the ORR, we expect an equivalent decrease of the activity. To check this, we horizontally shifted the data points of Pt(775), Pt(221), and Pt(331) (in Fig. 3.5c) to accommodate for the number of most active sites if all steps would be doubled. It is striking that the resulting data points (purple diamonds) fall now very close to the linear trend line, confirming again the importance of step bunching.

Finally, step bunching also impacts other structure-sensitive electrochemical reactions that are most active at step-related sites. Step bunches on Pt(111)-vicinals with n ≤ 5 show a reduced activity towards both the Hydrogen Oxidation Reaction [46] and the CO Oxidation Reaction [47]. By contrast, Nitrate Reduction shows a significant increase for n ≤ 5 [36], which suggests a more optimal binding of the reaction intermediates at the bunched steps.

Vacuum studies show that Pt(533), exhibiting (100) steps, undergoes step bunching during Ammonia Oxidation, resulting in a change in selectivity from producing N_2 to producing NO [48]. Moreover, in Chapter 4 we show that step bunching leads to a decrease of the hydrogen adsorption as well as platinum oxidation at step sites. To provide a graphical representation of our insights, we built up a stereographic triangle in which we indicate the surfaces that are unstable towards step bunching (see Fig. 3.5d and Appendix B). This is derived on the basis of the information in the literature regarding the electrochemical behavior of flame-annealed stepped platinum surfaces, together with this work and other characterization studies [24, 29, 30, 49, 50].

3.7 Conclusions

In this chapter we demonstrate that flame-annealed Pt(111)-vicinal electrodes with high step density undergo step bunching, which has a significant impact on the electrochemical behavior of the surface. Our statistical analysis of the terrace width and the step height distribution shows that, while Pt(554) presents a regular array of single steps separated by the nominal distance, 51±5 % and 14±3 % of the steps on Pt(553), which has higher step density, are bunched into pairs and triplets, respectively. This instability originates from the highly repulsive step-step interaction between closely distanced steps, which is lowered by forming step bunches with larger spacing in combination with a dipole moment that is increased only by ≈ 21 % to 0.17 D for double steps, in comparison to the 0.14 D of single steps. The bunching occurs during surface preparation at high temperature, when the surface mobility is enhanced. Pt(111)-vicinal electrodes with bunched steps exhibit an extra peak at around 0.185 V in the hydrogen desorption fingerprint, as well as an unexpected, non-linear trend of their E_{pztc} and ORR activity with their step density. Our new insight challenges the common assumption in electrochemistry that all vicinal surfaces present a regular array of monoatomic-height steps and can successfully explain the anomalous step density-dependent trends reported in literature.

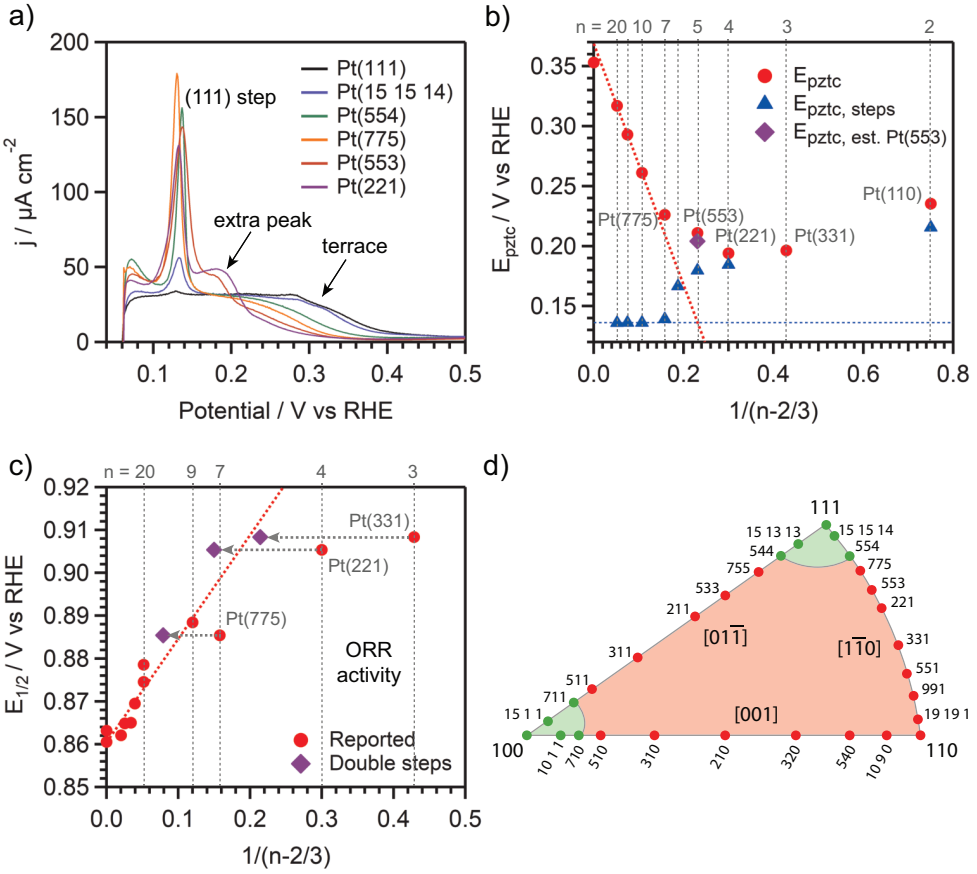

Figure 3.5: Effects of Step Bunching on Platinum Electrochemistry. **(a)** Hydrogen desorption fingerprint of Pt(111) and (111)-vicinal surfaces with (111) steps recorded in 0.1 M $HClO_4$ at a scan rate of 50 mV s^{-1}. The peaks related to terraces, single (111) steps, and step bunches, the latter only present on Pt(553) and Pt(221), are indicated. **(b)** E_{pztc} (in red) and (local) E_{pztc} at step sites (in blue) versus the step density, extracted from Refs. [7, 41, 43]. The stepped surfaces that undergo step bunching (n ≤ 7) do not follow the linear decrease of E_{pztc} with step density shown in red. The purple diamond represents our estimation of E_{pztc} for Pt(553), calculated from a fit of the dipole moment for double steps. **(c)** ORR activity, represented by the half-wave potential, versus step density, extracted from Refs. [8, 9]. The ORR activity increases linearly with the step density for n ≥ 9. The purple diamonds represent the adjusted values for Pt(775), Pt(221), and Pt(331) assuming that they only have double steps. **(d)** Stereographic triangle showing the stable surfaces in green and the unstable ones in red. Pt(110) forms a (1x2) missing-row reconstruction [24, 49], while Pt(100) is unreconstructed in electrolyte [50].

References

[1] B. Lang, R. W. Joyner, and G. A. Somorjai, *Surf. Sci.*, **30**, 454 (1972).

[2] D. W. Blakely and G. A. Somorjai, *Surf. Sci.*, **65**, 419 (1977).

[3] G. Comsa, G. Mechtersheimer, and B. Poelsema, *Surf. Sci.*, **119**, 159 (1982).

[4] E. Hahn, H. Schief, V. Marsico, A. Fricke, and K. Kern, *Phys. Rev. Lett.*, **72**, 3378 (1994).

[5] J. Clavilier, R. Faure, G. Guinet, and R. Durand, *J. Electroanal. Chem.*, **107**, 205 (1980).

[6] E. Herrero, J. M. Orts, A. Aldaz, and J. M. Feliu, *Surf. Sci.*, **440**, 259 (1999).

[7] V. Climent, R. Gómez, and J. M. Feliu, *Electrochim. Acta*, **45**, 629 (1999).

[8] A. Kuzume, E. Herrero, and J. M. Feliu, *J. Electroanal. Chem.*, **599**, 333 (2007).

[9] A. M. Gómez-Marín and J. M. Feliu, *Catal. Today*, **244**, 172 (2015).

[10] Y. I. Yanson, F. Schenkel, and M. J. Rost, *Rev. Sci. Instrum.*, **84**, 023702 (2013).

[11] M. J. Rost, in *Encyclopedia of Interfacial Chemistry*, 1st ed., K. Wandelt, p.180, Elsevier, Amsterdam (2018).

[12] L. Jacobse, Y. F. Huang, M. T. M. Koper, and M. J. Rost, *Nat. Mater.*, **17**, 277 (2018).

[13] E. D. Williams and N. C. Bartelt, *Science*, **251**, 393 (1991).

[14] H. Ibach, *Physics of Surfaces and Interfaces*, Springer, Amsterdam (2006).

[15] J. Lapujoulade, *Surf. Sci. Rep.*, **20**, 191 (1994).

[16] N. C. Bartelt, T. L. Einstein, and E. D. Williams, *Surf. Sci. Lett.*, **240**, L591 (1990).

[17] E. E. Gruber and W. W. Mullins, *J. Phys. Chem. Solids*, **28**, 875 (1967).

[18] R. Smoluchowski, *Phys. Rev.*, **60**, 661 (1941).

[19] C. Jayaprakash, C. Rottman, and W. F. Saam, *Phys. Rev. B*, **30**, 6549 (1984).

[20] K. H. Lau and W. Kohn, *Surf. Sci.*, **65**, 607 (1977).

[21] V. I. Marchenko and A. Ya. Parshin, *Sov. Phys. JETP*, **52**, 129 (1980).

[22] L. E. Shilkrot and D. J. Srolovitz, *Phys. Rev. B*, **53**, 122 (1996).

[23] G. Prévot, P. Steadman, and S. Ferrer *Phys. Rev. B*, **67**, 245409 (2003).

[24] K. Swamy, E. Bertel, and I. Vilfan, *Surf. Sci. Lett.*, **425**, L369 (1999).

[25] H. Jeong, E. D. Williams, *Surf. Sci. Rep.*, **34**, 171 (1999).

[26] J. Ikonomov, K. Starbova, H. Ibach, and M. Giesen, *Phys. Rev. Lett.*, **75**, 245411 (2007).

[27] R. C. Nelson, T. L. Einstein, and S. V. Khare, *Surf. Sci.*, **295**, 462 (1993).

[28] H. Ishida, A. Liebsch, *Phys. Rev. B*, **46**, 7153 (1992).

[29] A. Nakahara, M. Nakamura, K. Sumitani, O. Sakata, and N. Hoshi, *Langmuir*, **23**, 10879 (2007).

[30] N. Hoshi, M. Nakamura, O. Sakata, A. Nakahara, K. Naito, and H. Ogata, *Langmuir*, **27**, 4236 (2011).

[31] S. Baier, H. Ibach, and M. Giesen, *Surf. Sci.*, **573**, 17 (2004).

[32] H. Ibach and W. Schmickler, *Surf. Sci.*, **573**, 24 (2004).

[33] M. Giesen, G. Beltramo, S. Dieluweit, J. Müller, H. Ibach, and W. Schmickler, *Surf. Sci.*, **595**, 127 (2005).

[34] O. M. Magnussen, *Chem. Rev.*, **102**, 679 (2002).

[35] J. Clavilier, K. El Achi, and A. Rodes, *J. Electroanal. Chem.*, **272**, 253 (1989).

[36] S. Taguchi and J. M. Feliu, *Electrochim. Acta*, **52**, 6023 (2007).

[37] J. Souza-Garcia, V. Climent, and J. M. Feliu, *Electrochem. Commun.*, **11**, 1515 (2009).

[38] K. Besocke, B. Krahl-Urban, and H. Wagner, *Surf. Sci.*, **68**, 39 (1977).

[39] S. Trasatti, *J. Electroanal. Chem. Interf. Electrochem.*, **39**, 163 (1972).

[40] R. Gómez, V. Climent, J. M. Feliu, and M. J. Weaver, *J. Phys. Chem. B*, **104**, 597 (2000).

[41] R. Rizo, J. Fernández-Vidal, L. J. Hardwick, G. A. Attard, F. J. Vidal-Iglesias, V. Climent, E. Herrero, and J. M. Feliu, *Nat. Commun.*, **13**, 2550 (2022).

[42] P. N. Ross, *J. Chim. Phys.*, **88**, 1353 (1991).

[43] V. Climent, G. A. Attard, and J. M. Feliu, *J. Electroanal. Chem.*, **532**, 67 (2002).

[44] F. Calle-Vallejo, J. Tymoczko, V. Colic, Q. Huy Vu, M. D. Pohl, K. Morgenstern, D. Loffreda, P. Sautet, W. Schuhmann, and A. S. Bandarenka, *Science*, **350**, 185 (2015).

[45] F. Calle-Vallejo, M. D. Pohl, D. Reinisch, D. Loffreda, P. Sautet, and A. S. Bandarenka, *Chem. Sci.*, **8**, 2283 (2017).

[46] R. Kajiwara, Y. Asaumi, M. Nakamura, and N. Hoshi, *J. Elecroanal. Chem.*, **657**, 61 (2011).

[47] N. P. Lebedeva, M. T. M. Koper, J. M. Feliu, and R. A. van Santen, *J. Phys. Chem. B*, **106**, 12938 (2002).

[48] A. Scheibe, S. Günther, and R. Imbihl, *Catal. Letters*, **86**, 33 (2003).

[49] N. M. Marković, B. N. Grgur, C. A. Lucas, and P. N. Ross, *Surf. Sci.*, **384**, L805 (1997).

[50] L. A. Kibler, A. Cuesta, M. Kleinert, and D. M. Kolb, *J. Electroanal. Chem*, **484**, 73 (2000).